PAPER

A new route for laser cooling and trapping of cold molecules: Intensity-gradient cooling of MgF molecules using localized hollow beams

Kang Yan[1], Bin Wei[1] ⓘ, Yaling Yin[1] ⓘ, Supeng Xu[1], Liang Xu[2], Meng Xia[1], Ruoxi Gu[1], Yong Xia[1] ⓘ and Jianping Yin[1]

[1] State Key Laboratory of Precise Spectroscopy, School of Physics and Electronic Science, East China Normal University, Shanghai 200241, People's Republic of China
[2] Key Laboratory for Laser Plasmas (Ministry of Education) and School of Physics and Astronomy, Shanghai Jiao Tong University, Shanghai 200240, People's Republic of China

E-mail: ylyin@phy.ecnu.edu.cn and jpyin@phy.ecnu.edu.cn

Keywords: cold molecules, laser cooling, pure intensity-gradient cooing, localized hollow beam

Abstract

We propose a promising scheme to prepare ultracold MgF molecules from a slowed cold molecular beam by using three-dimensional pure intensity-gradient induced Sisyphus cooling. The cooling is based on a blue-detuned localized hollow beam and a weak repumping beam. We investigate the dynamic process in the trap with the method of the Monte-Carlo simulations, verifying the feasibility. Our results show that achieving sub-Doppler temperature should be possible in such a well-designed trap; the trapped MgF molecules with initial temperature of 1 mK can be directly cooled to the final equilibrium temperature of about 46.5 μK, well below the Doppler limit (about 527.9 μK for MgF); meanwhile, molecules with initial temperature of 14 mK can be even cooled to about 68.7 μK.

1. Introduction

For decades, many efforts have been made to produce a diverse set of dense ultracold molecular ensembles. Such ultracold molecular species provide magnificent platforms for the study of molecular science and it will greatly advance understandings in precision measurement, complex quantum systems under precise control, and ultracold chemistry in the most fundamental way [1–3]. Tremendous progress has been made in direct laser cooling and magneto-optical trap (MOT) of diatomic molecules, i.e. SrF [4–6], YO [7, 8] and CaF [9], or even polyatomic molecules SrOH [10]. CH_3F [11] and H_2CO [12] are also cooled by optoelectric Sisyphus cooling. In addition, some other ongoing candidates, such as YbF [13], BaF [14–16], and BaH [17], have attracted great interest as well. With Doppler cooling, the temperature of the laser-cooled molecules is usually much higher than the Doppler limit ($\hbar\Gamma/2k_B$) [18] due to its complex internal level structures [4, 7, 19], and the temperature can approach the Doppler limit as the laser intensity is reduced [6]. From [4, 20], we know that the type-I systems ($F' = F + 1$) is commonly used in laser cooling of atoms, where F is total angular momentum quantum number and the prime indicates the excited state. However, the cooling transition for molecules, where the rotational quantum number N' of the excited state is less than that of the ground state, is chosen to eliminate rotational branching, which introduces type-II systems ($F' = F$ or $F - 1$) and makes type-II transition inevitable. In the case of type-II systems, Doppler and sub-Doppler forces often have opposite sign, making the molecules be cooled to a relatively higher equilibrium temperature ($\sim$mK) [8, 21]. Sub-Doppler cooling, which can be generally understood from spatially varying polarization gradients in type-I systems, such as Sisyphus ($\pi_x - \pi_y$) and motion-induced orientation ($\sigma^+ - \sigma^-$) cooling [22, 23], is totally different in type-II systems, because of the existence of the dark states. There are two main cooling mechanisms in such transitions, the gray molasses and the magnetically-assisted Sisyphus cooling, both of which are able to cool particles to below the Doppler limit [24, 25]. On this basis, Truppe *et al* realized for the first time the cooling of molecules, well below the Doppler limit, using a three-dimensional blue-detuned molasses [26]. To date, the lowest

temperature was achieved by Λ-enhanced gray molasses and deep cooling with a single laser, both of which can cool CaF to several μK [27, 28]. Besides, laser cooling and deceleration of molecules with stimulated force has also progressed a lot both theoretically and experimentally [29–31].

As the common cooling method before molecules loaded into a type-II MOT, laser sweep slowing or white-light slowing, both of which are used to compensate Doppler shift, are not a very efficient way for larger number of molecules. This causes the problem of the small number and the low density of trapped molecules in the type-II MOT. In order to produce a diverse set of dense, ultracold diatomic molecular species, it would be interesting and worthwhile to explore how to produce much larger numbers of trapped molecules. Here we propose a new scheme for the preparation of ultracold molecules, which consists of the Stark-decelerated molecules and a localized hollow optical trap, where sub-Doppler cooling works well. We bypass the Doppler cooling, and achieve the process from supersonic molecular beam to sub-Doppler cooling of molecules. The localized hollow optical trap has a strong cooling capacity, and it can derive ultracold trapped molecules with higher density.

The cooling mechanism of a hollow optical trap is pure intensity-gradient cooling [32–37], another sub-Doppler cooling, which can also efficiently cool the molecules to the temperature of several photon recoils. The magnetic-field-assisted intensity-gradient cooling of molecules has first been observed in a one-dimensional standing wave, which have substantially reduced the transverse temperature of a SrF molecular beam [4]. Magnesium monofluoride (MgF) [38, 39], due to its highly diagonal Franck–Condon factors (FCFs) and strong spontaneous radiation decay, can also be a good candidate for laser cooling. Thus, it's necessary for us verify whether or not MgF is appropriate to intensity-gradient cooling. By virtue of intensity-gradient dipole force, we can cool and trap molecules in the well-designed trap.
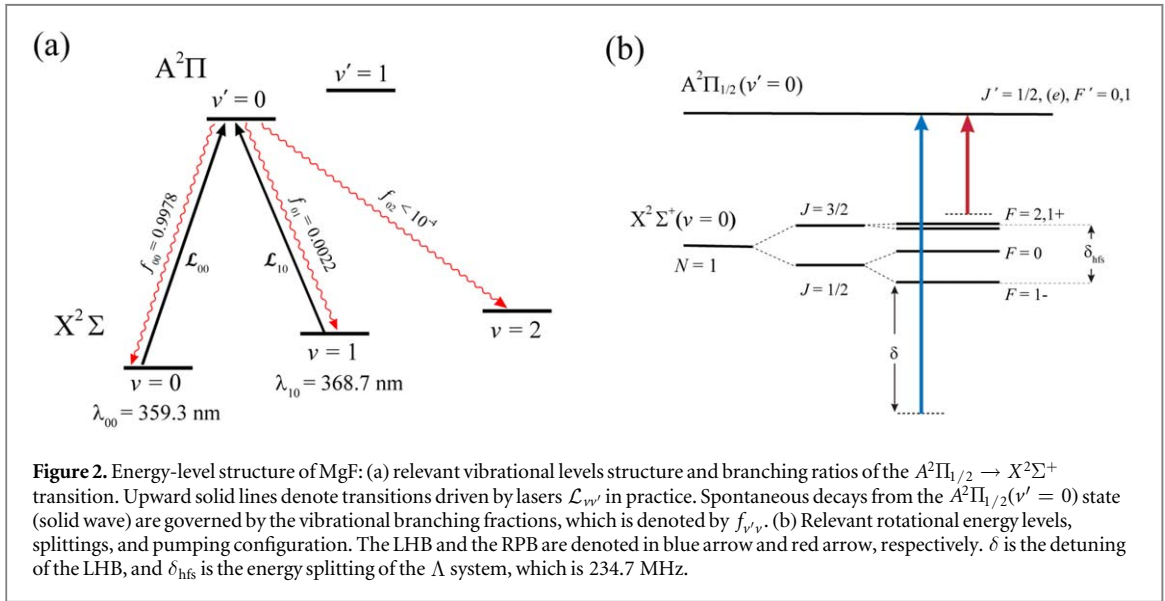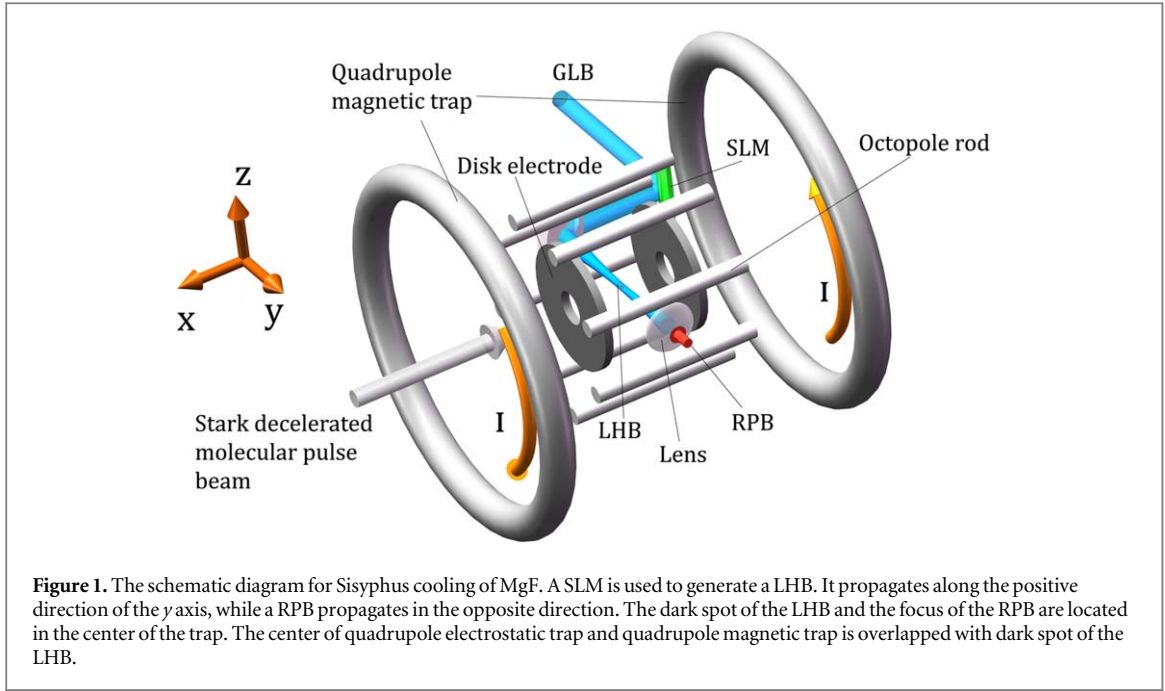
Here, we first propose the scheme to prepare ultracold MgF sample by using intensity-gradient cooling. In order to study the properties of intensity-gradient cooling, we consider two cooling lasers and a vibrational repumping laser. The cooling lasers contain a localized hollow beam (LHB) and a repumping beam (RPB). Because of the strong intensity-gradient force and low-rate spontaneous emission, the molecules in the LHB trap can be cooled to the lower temperature of several photon recoils. In the following, we will present how we construct the trap as well as the pumping configuration in section 2. Then, in section 3, we analyze the mechanism of heating and cooling in trap. At last, we perform three-dimension Monte-Carlo simulations for the dynamic process of the LHB-induced cooling, and obtain some new results and main conclusions.

2. Scheme for intensity-gradient cooling of MgF

2.1. Scheme
The scheme to trap and cool MgF molecules using a LHB and a weak RPB is shown in figure 1. The LHB is succinctly generated by a collimated Gaussian laser beam (GLB) and a spatial light modulator (SLM) [40]. There is a non-light area at the center of the generated LHB, which is dark spot (DS). The volume of the LHB, which is the ellipsoidal space enclosed by the maximum light intensity, can be effectively re-sized by changing parameters of the SLM. Two laser beams propagate along opposite directions on the optical axis (y axis).

In order to obtain much more pre-cooled molecules before loaded into the LHB trap, the scheme begins with the Stark deceleration of MgF molecules [41], and they are loaded into the LHB trap by two steps. First, the Stark decelerated MgF molecular package will be re-loaded for several times into a quadrupole electrostatic trap [42]. As shown in figure 1, the electrostatic trap consists of two disk electrodes with 4 mm diameter holes for the pulsed molecular beam passing through and eight cylindrical rods around forming an octopole. When applying the voltages of 0, $+U$ and $-U$ to the first disk electrode, the second one and the octopole, respectively, a loading-field configuration is formed. When the same voltage $+U$ is applied to the two disk electrodes and $-U$ is applied to the octopole, a trapping-field configuration is formed. As the Stark decelerated molecules enter the trap, the trap is switched into the loading-field configuration, then the molecules start to climb the potential hill and are slowed by the repulsive dipolar force. Upon the molecules are slowed to standstill near the trap center, the trap is switched into the trapping-field configuration, thus the molecules are confined in the electrostatic trap. We can repeat the loading and trapping process to obtain more trapped molecules. Second, after molecules are re-loaded into the electrostatic trap, we switch off the trap voltage, and then turn on the quadrupole magnetic trap, which consists of a pair of anti-Helmholtz coils [43]. The molecules clouds will be compressed by increasing the coil current. The compression will be continued until the MgF clouds are appropriate to be loaded into the LHB trap. This two steps are similar with the method used in. Reference [44], however, the re-loading of molecules in our scheme is finished in the electrostatic trap. By using the Monte-Carlo simulation, the total loading efficiency of cold MgF molecules from a supersonic molecular beam to the LHB trap is about 0.1%, with the temperature of about 10–14 mK. If the flux of the supersonic MgF beam is about the order of 10^9–10^{10} molecules/steradian/pulse [45–49], the trapped cold MgF number is estimated by about 10^6–10^7 and its density can reach to about 10^{10}–10^{11} cm^{-3}.

Figure 1. The schematic diagram for Sisyphus cooling of MgF. A SLM is used to generate a LHB. It propagates along the positive direction of the *y* axis, while a RPB propagates in the opposite direction. The dark spot of the LHB and the focus of the RPB are located in the center of the trap. The center of quadrupole electrostatic trap and quadrupole magnetic trap is overlapped with dark spot of the LHB.

Figure 2. Energy-level structure of MgF: (a) relevant vibrational levels structure and branching ratios of the $A^2\Pi_{1/2} \rightarrow X^2\Sigma^+$ transition. Upward solid lines denote transitions driven by lasers $\mathcal{L}_{vv'}$ in practice. Spontaneous decays from the $A^2\Pi_{1/2}(v'=0)$ state (solid wave) are governed by the vibrational branching fractions, which is denoted by $f_{v'v}$. (b) Relevant rotational energy levels, splittings, and pumping configuration. The LHB and the RPB are denoted in blue arrow and red arrow, respectively. δ is the detuning of the LHB, and δ_{hfs} is the energy splitting of the Λ system, which is 234.7 MHz.
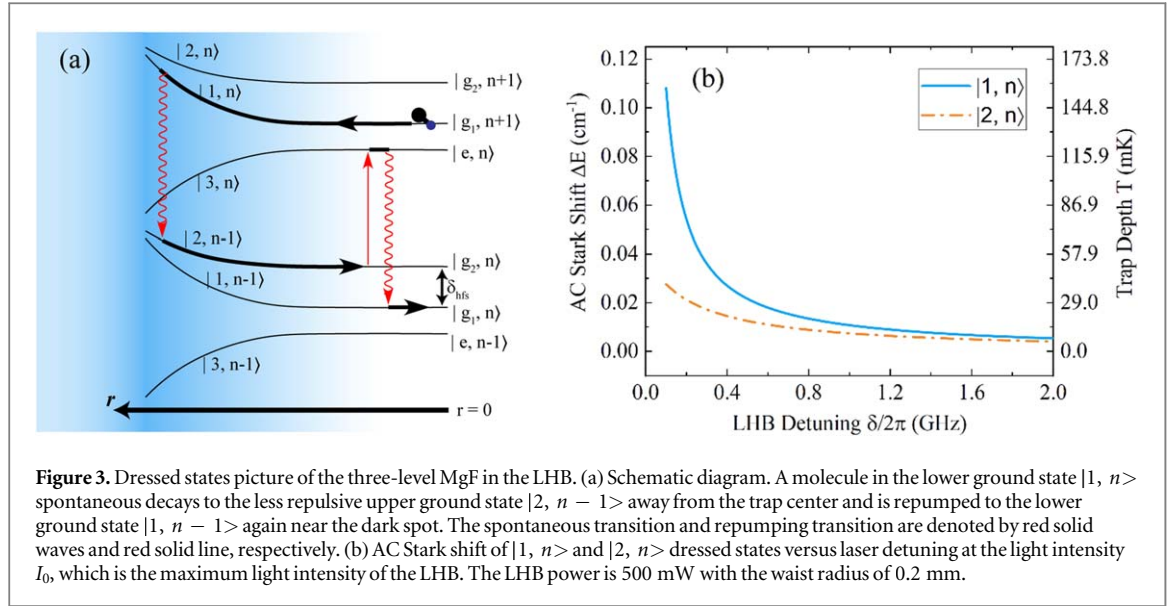
After that, the loaded cold molecules can be trapped if the kinetic energy is lower than the trap depth of the LHB. Then, the cold molecules will experience intensity-gradient induced Sisyphus cooling provided by the LHB and the weak RPB (see section 3), which can compensate the heating of the molecules in the LHB resulting from the spontaneous emission. Finally, the ultracold molecules will be prepared in the LHB trap after a period of cooling time.

2.2. Level structure of MgF for cooling

In this section, we analyze the energy level structure of the MgF molecule needed for the intensity-gradient cooling scheme. There is no selection rule for vibrational transitions between electronic dipole transitions, the transition intensity of which is determined by FCFs, which describes the relative rates of spontaneous decaying from an excited electronic state into ground electronic state with vibrational quantum numbers v' and v, respectively. For MgF [38], its highly diagonal FCFs and strong spontaneous decay rate make it appropriate for our scheme. As shown in figure 2(a), the laser denoted by $\mathcal{L}_{vv'}$ (corresponding wavelength is $\lambda_{vv'}$) drives the $X^2\Sigma^+(v) \rightarrow A^2\Pi_{1/2}(v')$ transition, and $\mathcal{L}_{00}$ denotes the cooling lasers, which consists of a LHB and a RPB, while $\mathcal{L}_{10}$ is the vibrational RPB.

We choose a ground state $X^2\Sigma^+(v=0,\ N=1)$ and drive a transition to an excited state $A^2\Pi_{1/2}(v'=0,\ J'=1/2)$. As shown in figure 2(b), the ground state is split into $J=1/2,\ 3/2$ levels through spin-rotation

Figure 3. Dressed states picture of the three-level MgF in the LHB. (a) Schematic diagram. A molecule in the lower ground state $|1, n>$ spontaneous decays to the less repulsive upper ground state $|2, n − 1>$ away from the trap center and is repumped to the lower ground state $|1, n − 1>$ again near the dark spot. The spontaneous transition and repumping transition are denoted by red solid waves and red solid line, respectively. (b) AC Stark shift of $|1, n>$ and $|2, n>$ dressed states versus laser detuning at the light intensity I_0, which is the maximum light intensity of the LHB. The LHB power is 500 mW with the waist radius of 0.2 mm.

interaction, then splits into $F = 1^−$, 0, 1^+, 2 because of the nuclear spin $I = 1/2$, where $F = 1^\pm$ denote the upper and lower $F = 1$ energy level. The LHB is blue detuned from the frequency of the $X^2\Sigma^+(N = 1, F = 1^−) \rightarrow A^2\Pi_{1/2}(J' = 1/2(e))$ transition, with the detuning denoted δ, while the weak RPB is red detuned from the frequency of the $X^2\Sigma^+(N = 1, F = 2) \rightarrow A^2\Pi_{1/2}(J' = 1/2(e))$ transition. In addition, in constructing a Λ system, the degenerate state consists of $F = 2$, 1^+ is the upper ground state, since the energy splitting between $F = 2$, 1^+ is only 9.3 MHz, which is small compared to the natural linewidth of 22 MHz and is much smaller than the LHB detuning. The hyperfine $F = 1^−$ state is the lower ground state. The left $F = 0$ state in the middle can be negligible in the far detuned pumping configuration since the population accumulated in that state is extremely small and has been experimentally proved in [27], where they neglect the effect of $F = 0$ state of CaF in the case of non-near resonance.

In order to remix dark Zeeman sublevels $|F = 2, M_F = \pm2\rangle$, we apply a magnetic field B_0 at angle of $\theta_B = 45°$ relative to the laser polarization. Thus the dark Zeeman sublevels are eliminated because Larmor precession will bring dark states into the bright states with angular frequency $\omega_B \sim g_F \mu_B B_0$, where g_F of $F = 2$ is about 0.5 [39]. The vibrational RPB $\mathcal{L}_{10}$ is required to repump molecules back to $\nu = 0$ state in practice, however, the impacts of them on cooling effect are much smaller than that of the LHB. Since the LHB is far detuned from electronic transition frequency, the population in $\nu = 0$ state is much larger than that in $\nu' = 0$ state if we set the laser power of the LHB and $\mathcal{L}_{10}$ as the same. In the simulation, we consider the influence of vibrational repumping on the cooling effect. So, such pumping configuration consisted of a LHB and a RPB construct a quasi-closed transition cycle.

3. Model of intensity-gradient induced Sisyphus cooling of MgF

3.1. Dressed states and spontaneous transition
In this section, we will give the semiclassical description of the interaction of cold MgF molecules with cooling lights as follows. Since we consider a three-level MgF model, the exited state $|e\rangle$ and two ground states $|g_1\rangle$ and $|g_2\rangle$, corresponding to the $|J' = 1/2(e)\rangle$ state, the hyperfine structures $|N = 1, F = 1^−\rangle$ and $|N = 1, F = 1^+, 2\rangle$, respectively. The states $|g_1, n + 1\rangle$, $|g_2, n + 1\rangle$ and $|e, n\rangle$ with $n + 1$ and n LHB photons are coupled to each other, which forms a ladder of dressed state multiples, labeled as $|1, n\rangle$, $|2, n\rangle$ and $|3, n\rangle$. And they are separated from neighboring multiples by the photon energy (see figure 3(a)). The corresponding optical potentials (or called AC Stark shift) are U_1, U_2 and U_3, respectively, where $U_3 = −U_1 − U_2$ (please see appendix A). The optical potential U_i of $|1, n>$ and $|2, n>$ is repulsive when the LHB is blue-detuned, shown in figure 3(b), and U_i varies spatially because of the light intensity distribution of the LHB.

Due to the dressed state $|1, n\rangle$ containing a small admixture of the excited state, it may decay to a lower dressed state multiples $|i, n − 1\rangle$, as shown in figure 3(a). The scattering rates of these spontaneous transitions depend on the saturation parameter s, which varies in the different location of the LHB. They can be written as follows [32]:

$$\Gamma_{11} \approx q_{LHB}\Gamma s/3, \tag{1}$$

$$\Gamma_{12} \approx (1 − q_{LHB})\Gamma s/3, \tag{2}$$

$$\Gamma_{13} \approx [1 + \delta^2/(\delta + \delta_{\mathrm{hfs}})^2]\, \Gamma(s/3)^2, \tag{3}$$

where Γ_{1i} is the spontaneous decay rate from $|1, n\rangle$ to $|i, n-1\rangle$, q_{LHB} is the mean branching ratio to the lower ground states after scattering a LHB photon, $s = (\Omega^2/2)/(\delta^2 + \Gamma^4/4)$. Ω is the Rabi frequency, $\Omega = \sqrt{I/2I_{\mathrm{sat}}}\,\Gamma$, where $I_{\mathrm{sat}} = (\pi h c \Gamma)/(3\lambda^3)$. The exact arithmetic solution of LHB laser intensity profile is presented in [40], and the approximate analytic solution used in the simulation is $I(r, a) = I_0 \exp\left(-2(\sqrt{r^2 + (R \times a)^2} - r_0)^2/w^2\right)$, where r and a are radial component and axial component, respectively, R is the ratio of the long axis to the short axis, r_0 is the radial size of LHB, w is the full width at half maximum of a single peak of radial intensity distribution at $a = 0$ plane. The total scattering rate P_{sp} can be obtained, i.e. $P_{\mathrm{sp}} = 1 - \exp\left(-\int (\Gamma s/3)\mathrm{d}t\right)$ [32].

3.2. Mechanism of cooling and heating

In the blue-detuned LHB trap, a molecule in $|g_1, n+1\rangle$ ground state that moves along the repulsive optical potential U_1 from the center of DS will be adiabatically evolved into the dressed state $|1, n\rangle$. The molecule then is decelerated due to repulsive potential U_1. During the previous process, it may absorb a LHB photon and emit a fluorescent photon in a random direction, spontaneously decaying into the upper fine dressed state $|2, n-1\rangle$ with the rate of $(1 - q_{\mathrm{LHB}})P_{\mathrm{sp}}$, which results in a small heating by two recoil energies E_R,

$$\int_0^\infty 2E_R \Gamma_{12}\mathrm{d}t = 2(1 - q_{\mathrm{LHB}})E_R P_{\mathrm{sp}}, \tag{4}$$

where $E_R = (\hbar k)^2/2m$, Γ_{12} is the spontaneous decay rate from $|1, n\rangle$ to $|2, n-1\rangle$. For MgF, $q_{\mathrm{LHB}} \approx 0.497$ (please see appendix B).

After that, it moves back to the DS along the potential U_2, losing part of its kinetic energy since the potential U_2 of $|2, n-1\rangle$ state is less repulsive than U_1 of $|1, n\rangle$. The kinetic energy loss is proportional to the difference between the optical potential of the two dressed states, i.e. $\Delta U = U_1 - U_2$, which is Sisyphus cooling effect

$$\int_0^\infty (U_1 - U_2)\Gamma_{12}\mathrm{d}t = -\frac{2}{3}\frac{U_2}{U_1}E_\perp(1 - q_{\mathrm{LHB}})P_{\mathrm{sp}}, \tag{5}$$

where $E_\perp = m v_\perp^2/2$, $v_\perp$ is the velocity component of a molecule perpendicular to the LHB direction.

When the molecule approaches the DS, it may be repumped back to the lower fine dressed state $|1, n-1\rangle$ (see figure 3(a)) if it is in the range of the weak RPB. Therefore, a closed and repeatable LHB-induced Sisyphus cooling cycle is formed. During the repumping process, it absorbs a RPB photon and then spontaneous emits a fluorescent photon, which results in a small heating by two recoil energies

$$\int_0^\infty 2E_R \Gamma_{12}\mathrm{d}t = 2E_R\frac{1 - q_{\mathrm{LHB}}}{q_{\mathrm{RPB}}}P_{\mathrm{sp}}, \tag{6}$$

where q_{RPB} is the mean branching ration into the lower ground state for the excitation of the upper ground state by the RPB. For MgF, $q_{\mathrm{RPB}} \approx 0.369$ (please see appendix B).

Besides the $|1, n\rangle \to |2, n-1\rangle$ transition mentioned above, there are two spontaneous emission channels as follows.

(1) The $|1, n\rangle \to |1, n-1\rangle$ transition leads to a small heating with the rate of $q_{\mathrm{LHB}}P_{\mathrm{sp}}$,

$$\int_0^\infty 2E_R \Gamma_{11}\mathrm{d}t = 2E_R q_{\mathrm{LHB}}P_{\mathrm{sp}}, \tag{7}$$

(2) The $|1, n\rangle \to |3, n-1\rangle$ transition results in a heating because the molecule in $|3, n-1\rangle$ is accelerated by the attractive potential. However the corresponding rate ($P_{1\to3} \approx (2E_\perp P_{\mathrm{sp}})/(3\hbar\delta) \ll P_{\mathrm{sp}}$) is so small that can be neglected. Now we take all the cooling and heating effects into consideration and give the equilibrium equation used to evaluate the rms momentum P_{rms},

$$-\frac{1}{3}\frac{U_2}{U_1}\left(\frac{P_{\mathrm{rms}}}{\hbar k}\right)^2 + \frac{1}{q_{\mathrm{RPB}}} + \frac{q_{\mathrm{LHB}}}{1 - q_{\mathrm{LHB}}} = 0. \tag{8}$$

4. Monte-Carlo simulations and results

To investigate the effect of the intensity-gradient induced Sisyphus cooling of MgF in the LHB trap, we present a quantitative study by using three-dimension Monte-Carlo simulation, and the results are shown in figures 4–7. For MgF, the natural linewidth Γ and the saturation intensity I_{sat} are $2\pi \times 22$ MHz and 62.7 mW cm^{-2}, respectively. The radial and axial lengths of the LHB in the focus plane are $w_{r\mathrm{LHB}} = 100$ μm and $w_{a\mathrm{LHB}} = 500$ μm, the volume of which is $V_{\mathrm{LHB}} = (4\pi w_{r\mathrm{LHB}}^2 w_{a\mathrm{LHB}})/3 \approx 2.1 \times 10^{-11}$ m^3 and can be re-sized.
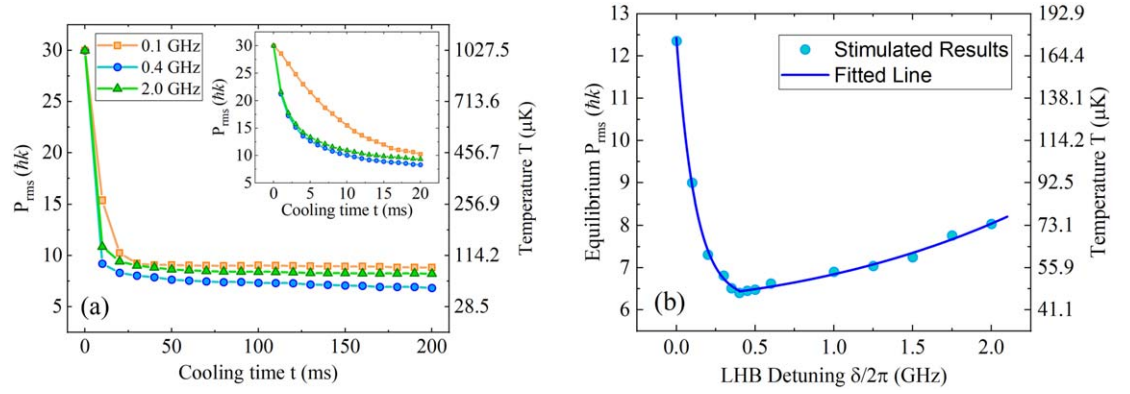
Figure 4. The results of Monte-Carlo simulation related to laser detuning of the LHB. (a) The time evolution of rms momentum P_{rms} and the corresponding temperature of trapped MgF molecules for different laser detuning $\delta/2\pi$. (b) The final equilibrium rms momentum and temperature of MgF versus the laser detuning of the LHB. For all plots, LHB power $P_0 = 500$ mW, RPB power $RP_0 = 0.06$ mW, the LHB volume $V_{LHB} \approx 2.1 \times 10^{-11}$ m^3 ($w_{rLHB} = 100$ μm) and the RPB volume $V_{RPB} \approx 4.5 \times 10^{-12}$ m^3 ($w_{rRPB} = 60$ μm).
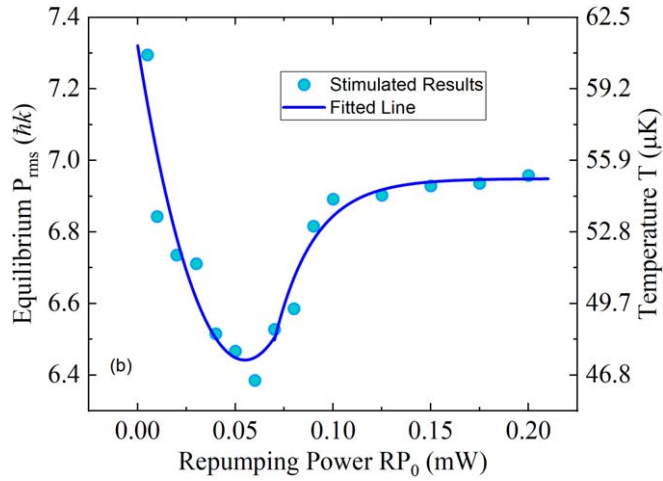
Figure 5. The final equilibrium rms momentum P_{rms} and the corresponding temperature of MgF versus the RPB power RP_0. We fix $\delta/2\pi$ at 0.4 GHz, and other parameters in the simulation are the same as figure 4.
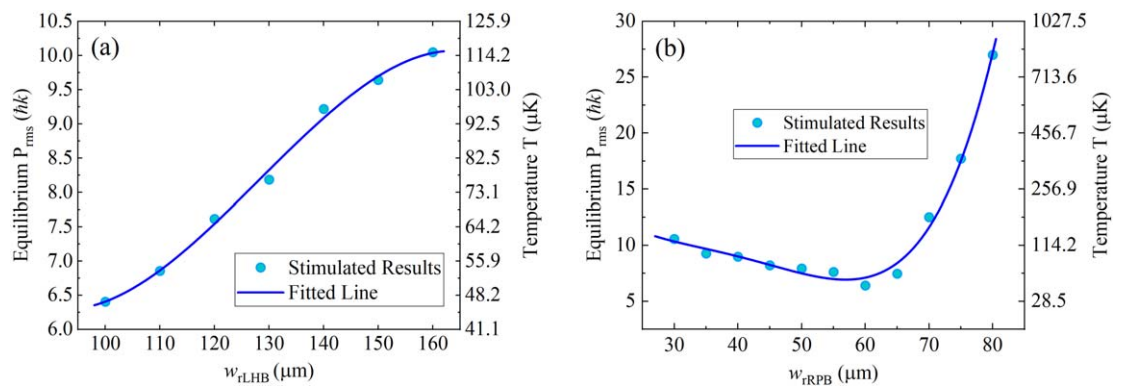
Figure 6. The final equilibrium rms momentum P_{rms} and the corresponding temperature of MgF versus the radius of LHB and RPB at the focus plane. (a) The radius of LHB ranges from $w_{rLHB} = 100$ to 160 μm, corresponding volume of the LHB from 2.1×10^{-11} to 8.6×10^{-11} m^3, respectively, and w_{rRPB} is fixed at 60 μm. (b) The radius of RPB is from $w_{rRPB} = 30$ to 80 μm, corresponding volume of the LHB from 5.7×10^{-13} to 1.1×10^{-11} m^3, respectively, and w_{rLHB} is fixed at 100 μm. For all plots, LHB power $P_0 = 500$ mW, RPB power $RP_0 = 0.06$ mW, the LHB detuning $\delta/2\pi = 0.4$ GHz.
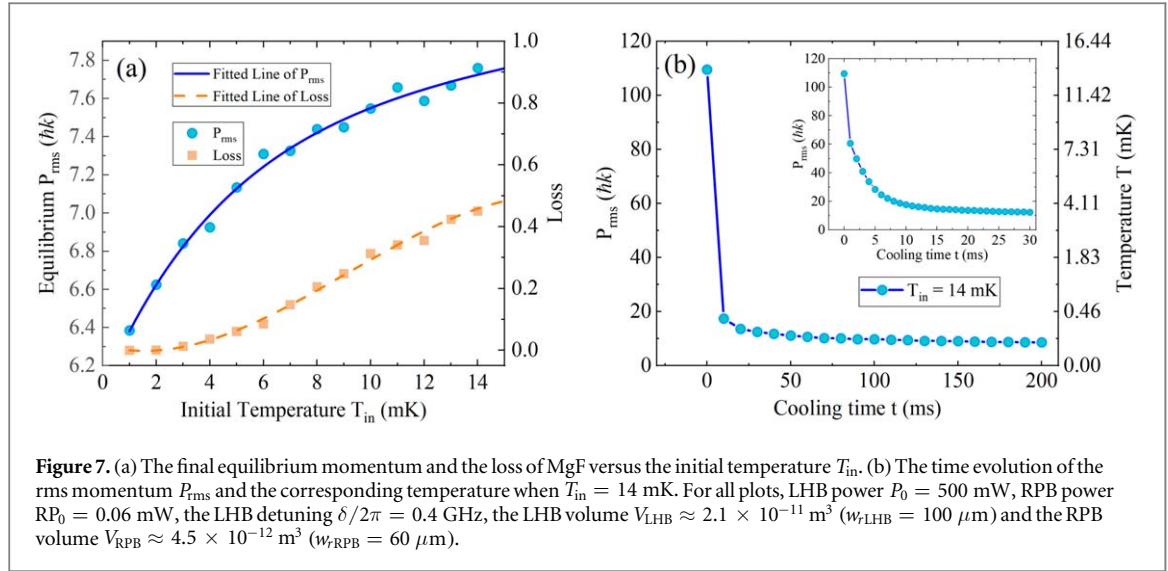
Figure 7. (a) The final equilibrium momentum and the loss of MgF versus the initial temperature T_{in}. (b) The time evolution of the rms momentum P_{rms} and the corresponding temperature when $T_{in} = 14$ mK. For all plots, LHB power $P_0 = 500$ mW, RPB power $RP_0 = 0.06$ mW, the LHB detuning $\delta/2\pi = 0.4$ GHz, the LHB volume $V_{LHB} \approx 2.1 \times 10^{-11}$ m^3 ($w_{rLHB} = 100$ μm) and the RPB volume $V_{RPB} \approx 4.5 \times 10^{-12}$ m^3 ($w_{rRPB} = 60$ μm).

Here, we will discuss how the volume of the LHB and the RPB affects the cooling results. The wavelength of the GLB is 359.3 nm and its laser power is 500 mW with the waist radius of 0.2 mm. When $\delta/2\pi = 0.4$ GHz, the corresponding trap depth of the LHB for the $|1, n\rangle$ state and the $|2, n-1\rangle$ state is 39.15 mK and 21.05 mK, respectively. The trap depth is high enough to trap the molecules with a temperature of ~ 14 mK as long as the magnetic field we applied can efficiently remix the dark states.

In order to optimize all the parameter, we first fix the initial rms momentum of the molecules at $P_{in} \approx 30$ $\hbar k$, whose corresponding temperature is $T_{in} \approx 1$ mK. In the simulation, we take the mechanism of remixing dark states into account. When MgF molecules spontaneously decay to the upper ground dressed state $|2, n-1\rangle$, they may fall into the dark states, where molecules do not subject to a repulsive force since there is no AC Stark shift for them. In the presence of external magnetic field B, the dark states $|F = 2, M_F = \pm 2\rangle$ will be brought into bright ones while the bright states $|F = 2, M_F = \pm 1, 0\rangle$ in $|2, n-1\rangle$ will evolve into dark ones, the rate of which depends on the Larmor frequency. Therefore, the magnitude of B will influence the cooling efficiency, or at least, B should ensure that the loss is as small as possible. We find that loss decreases drastically with magnetic field when magnetic field $B < 0.4$ G. In the case of $B > 0.4$ G, almost all the molecules with the initial temperature of 1 mK do not escape from the trap, and cooling efficiency do not change much with different magnetic field. So we fix the magnetic field B at 1.0 G in the following simulations, which is enough to efficiently remix dark states.

After fixing the magnetic field, we study the time evolution of the rms momentum of the MgF molecules for different laser detuning, and the results are shown in figure 4(a). The conclusions are given as follows: (1) The rms momentum of the cooled molecules decreases quickly at the beginning of the time evolution, then the cooling is almost completed after a cooling period of 20 ms. There is a dynamical equilibrium between the Sisyphus cooling effect and the heating one, which results from scattering a LHB photon or a RPB one. (2) The laser detuning of the LHB will influence the final equilibrium rms momentum. When $\delta/2\pi = 0.4$ GHz, the final rms momentum of the cooled MgF molecules in the LHB trap can reach $P_{rms} \approx 6.39$ $\hbar k$ (the theoretical value 4.8 $\hbar k$ derived from equation (8)) and the corresponding temperature is ~ 46.5 μK. In the case of $\delta/2\pi = 0.1$ GHz, the final rms momentum is $P_{rms} \approx 9.03$ $\hbar k$ and the corresponding temperature is ~ 93.1 μK. When $\delta/2\pi = 2$ GHz, the final rms momentum is $P_{rms} \approx 8.09$ $\hbar k$ and the corresponding temperature is ~ 73.7 μK. All final equilibrium momentum are statistical averages between 200 and 500 ms. The results show that the MgF with the temperature of ~ 1 mK can be efficiently cooled down to ~ 46.5 μK in our LHB trap, and P_{rms} varies with different laser detuning.

Next, we show how the final equilibrium rms momentum P_{rms} depends on the laser detuning of the LHB, and the results are shown in figure 4(b). The laser power of the LHB and the RPB is fixed at $P_0 = 500$ mW and $RP_0 = 0.06$ mW, respectively, and we only change the value of the detuning. It is evident that: (1) There is an optimal parameter with $\delta/2\pi = 0.4$ GHz and the corresponding final equilibrium momentum is $P_{rms} \approx 6.39$ $\hbar k$ (corresponding to 46.5 μK). (2) When the laser detuning is less than 0.4 GHz, the final equilibrium rms momentum decreases drastically with the increase of the detuning. This is because the spontaneous heating effects resulting from scattering a LHB photon or a RPB one are much larger than the Sisyphus cooling effect in the case of small detuning. The smaller the laser detuning is, the higher the heating rate is, and the heating rate increases faster than the cooling one as the detuning decreases. Thus, this will result in a

drastic decrease with the detuning ranging from 0 to 0.4 GHz. (3) When it comes to the larger detuning, the final equilibrium momentum increases with the detuning ranging from 0.4 to 2 GHz. The reason is that the kinetic energy loss during each cycle of Sisyphus cooling will decrease, which results in the reduction of the intensity-gradient induced cooling efficiency. The heating effect resulting from the scattering a light field photon also reduces with the detuning. However, the reduction of heating rate is slower than that of the cooling one. Thus the equilibrium temperature of the molecules will increase with the laser detuning. The results in figure 4(a) also show that the evolution time of the rms momentum of the cooled MgF in an intensity-gradient LHB trap is basically independent of the laser detuning.

Besides, we investigate the influence of different RPB power (RP$_0$) on the final equilibrium rms momentum. The results are shown in figure 5. It is clear that the final equilibrium rms momentum can reach $P_{rms} \approx 6.39\ \hbar k$ and the corresponding temperature is $\sim$46.5 μK when the RP$_0$ is $\sim$0.06 mW, which is the optimal parameter. The explanation is that both the Sisyphus cooling rate and the spontaneous-emission one are dependent on the laser power of the RPB. When the RPB power is weaker, the molecules in a dressed state $|2, n - 1\rangle$ are less likely to absorb a RPB photon, which results in the reduction of the intensity-gradient induced cooling cycles. This means that the cooling rate will decrease. Then the reduction of the cooling rate is followed by the increase of the final equilibrium rms momentum. However, the higher the RPB power is, the more significant the spontaneous-emission heating effect is. And the heating effect will saturate if the RPB power is much higher. The optimal RPB power will be obtained when there is a balance between the cooling effect and the heating one.

The size of the LHB trap and the RPB are important for our scheme. Then we investigate the relationship between the final equilibrium rms momentum P_{rms} and the volumes of both the LHB trap and the RPB. Figure 6(a) shows that P_{rms} increases slowly with the LHB trap volume. This is because the intensity gradient of the LHB trap reduces with the increasing of trap size, which results in the reduction of the intensity-gradient cooling effect.

As shown in figure 6(b), the equilibrium rms momentum P_{rms} first slowly decreases with the RPB volume then drastically increases from $w_{rRPB} = 70$ to 80 μm. The explanation is given as follows. The mechanism of intensity-gradient induced cooling actually takes advantage of the fact that the optical gradient forces of various dressed states are different and the difference varies spatially in the trap. If the repumping region is bigger, the molecules in $|2, n - 1\rangle$ state are more likely to be repumped to the $|1, n - 1\rangle$ state ahead of time. And the molecules will move a shorter distance back to the DS along the repulsive potential U_2 ($U_2 < U_1$). Thus, the bigger the repumping region is, the less the kinetic energy loss at a time is, which results in the reduction of cooling rate. However, the dark Zeeman sublevels of the $|2, n - 1\rangle$ state will weaken the rate of scattering a RPB photon, and the Sisyphus cooling effect will be reduced if the repumping region is small. As a result, there is an optimal waist radius $w_{rRPB} \approx 60$ μm and the cooling effect will be worse when $w_{rRPB} > 60$ μm. We also find that when $w_{rRPB} \gtrsim 70$ μm, the final equilibrium rms momentum drastically increases. We calculate the radial optical gradient force of the $|1, n\rangle$ state with $P_0 = 500$ mW and $\delta = 2\pi \times 0.4$ GHz, the maximum force is 1.1×10^{-23} N at the radial direction of $r \approx 70$ μm, which could explain the results mentioned above. Thus the cooling effect is strongly dependent on the RPB volume and $V_{RPB} < V_{LHB}$ is a condition to construct efficient intensity-gradient induced Sisyphus cooling.

Till now, we have optimized all the parameters. Finally, we study the dependence of the final equilibrium temperature of trapped molecules on initial temperature, ranging from $T_{in} \approx 1$ to 14 mK. The results are shown in figure 7. We find that the trapped molecules with the initial temperature of $T_{in} \approx 1$ mK can be cooled down to $T \approx 46.5$ μK, whose equilibrium momentum is $P_{rms} \approx 6.39\ \hbar k$. From figure 7(a), it is obvious that the final equilibrium temperature of trapped MgF molecules increases with the initial temperature. In the case of $P_0 = 500$ mW, the trap depth of the dressed state $|2, n - 1\rangle$ is about 21 mK, but the trapping effect is weakened because of the influence of the dark states. When the initial temperature approaches the trap depth, only colder molecules will not escape, which causes the final equilibrium temperature curve to flatten out. The trapped molecules with the initial temperature of $T_{in} \approx 14$ mK can be cooled down to $T \approx 68.7$ μK, corresponding equilibrium momentum is $P_{rms} \approx 7.8\ \hbar k$. Figure 7(a) also shows that the loss increases with the initial temperature of trapped molecules, and the loss of $T_{in} \approx 1$ mK is almost zero while that of $T_{in} \approx 14$ mK is about 0.45, which can be further reduced by increasing the power of the LHB. As shown in figure 7(b), when the starting temperature is 14 mK, the cooling is almost complete within 50 ms, and the trapped molecules scatter $\sim$30 photons within 1 ms. Considering the loss of LHB, the number of trapped MgF molecules is $\sim 10^6 - 10^7$, and estimated density is $\sim 10^{10} - 10^{11}$ cm^{-3}, with the temperature of $\sim$68.7 μK.

5. Conclusion

Let us now summarize our findings. Our simulation results show that in the blue-detuned LHB trap the molecules with the initial temperature of 1 mK can be directly cooled to $\sim$46.5 μK, and the corresponding final

rms momentum is 6.39 $\hbar k$. We also find that the intensity-gradient Sisyphus cooling effect of trapped MgF molecules depends on both the laser detuning of the LHB and the laser power of the RPB. The corresponding optimal parameters are $\delta/2\pi = 0.4$ GHz and $RP_0 = 0.06$ mW when the LHB power is $P_0 = 500$ mW. In order to guarantee the cooling effect, the volume of LHB should be bigger than that of RPB, and the suggested ratio is $V_{LHB}/V_{RPB} \approx 4.6$ ($w_{rLHB} = 100\ \mu$m, $w_{rRPB} = 60\ \mu$m). In such trap, the molecules with the initial temperature of ~ 14 mK can be even cooled to $\sim 68.7\ \mu$K (7.8 $\hbar k$) with the loss of 0.45 and the number of trapped MgF molecules is $\sim 10^6 - 10^7$, and estimated density is $\sim 10^{10} - 10^{11}$ cm^{-3}. As a result, the intensity-gradient induced Sisyphus cooling in our scheme can be used to efficiently trap and cool MgF molecules. Our scheme bypasses the traditional route, which consists of Doppler laser cooling and a type-II MOT stage. The trap depth of a MgF-MOT is about 1 K [39], and the depth of our LHB trap is about several tens mK. But the depth of the LHB trap is enough to capture the prepared cold molecules by Stark deceleration and magnetic field compression, which are cooled efficiently by intensity-gradient cooling. By virtue of the mechanism of the sub-Doppler cooling, the molecules in the LHB trap can be cooled well below the Doppler limit, even approaching the temperature of several photon recoils. Thus, our scheme bridges the gap between Stark decelerated supersonic beam and sub-Doppler temperature. And compared with a red- or blue-detuned MOT, the ultracold molecules can also be obtained with higher density in the LHB trap because of its smaller and tunable trapping volume.

Acknowledgments

Appendix A

We calculate the AC Stark shifts of the hyperfine energy levels in $^2\Sigma$ state for the Hunds case (b) to Hunds case (a) molecular transitions of the $^2\Sigma$–$^2\Pi$ form, and the method we used is perturbation theory. The effect of the multilevel structure of molecules on their response to an electromagnetic field may be conveniently described with the help of the electric dipole polarizability. Here $|\varphi_\kappa\rangle = |\kappa,\ n\rangle$ is specific molecular state of interest, where n denotes the photon number. In the follow discussion, n is not important because the Stark shift of the $|\kappa,\ n\rangle$ state is exactly the same as any $|\kappa,\ m\rangle$ state. Since there are no diagonal matrix elements of the electric dipole interaction, $\langle\varphi_\kappa|\ T_p^1(d)\ \cdot\ \hat{e}|\varphi_\kappa\rangle = 0$, which means there is no first-order correction to the energy. However, the external light field will cause the second-order correction to the energy of the $|\varphi_\kappa\rangle$ state, which is the AC Stark shift [50]

$$U_\kappa = \Delta E_\kappa = -\frac{\xi^2}{4}\sum_\beta\left\{\left(\frac{1}{\epsilon_\kappa - \epsilon_\beta - \hbar\omega} + \frac{1}{\epsilon_\kappa - \epsilon_\beta + \hbar\omega}\right)|\langle\varphi_\kappa|\ T_p^1(d)\ \cdot\ \hat{e}|\varphi_\beta\rangle|^2\right\}, \tag{A.1}$$

where the sum is over all molecular states $|\varphi_\beta\rangle$ that directly coupled to the $|\varphi_\kappa\rangle$ state and ξ donates the electric field amplitude. The dynamic polarizability operator can be written as follows

$$\alpha_{\gamma,\gamma'}(\omega) = \sum_\beta\left\{\left(\frac{1}{\epsilon_\kappa - \epsilon_\beta - \hbar\omega} + \frac{1}{\epsilon_\kappa - \epsilon_\beta + \hbar\omega}\right)d_\gamma^*|\varphi_\beta\rangle\langle\varphi_\beta|\ d_{\gamma'}\right\}, \tag{A.2}$$

where $\alpha_{\gamma,\gamma'}(\omega)$ is dependent on ω and $d_\gamma = T_p^1(d)\ \cdot\ \hat{e}$ are the Cartesian components of the dipole moment operator in the space-fixed coordinate frame. Then equation (A.1) becomes

$$U_\kappa = \Delta E_\kappa = -\frac{\xi^2}{4}\langle\varphi_\kappa|\alpha_{\gamma,\gamma'}|\ \varphi_\kappa\rangle = -\frac{\xi^2}{4}\sum_\beta\left\{\left(\frac{1}{\epsilon_\kappa - \epsilon_\beta - \hbar\omega} + \frac{1}{\epsilon_\kappa - \epsilon_\beta + \hbar\omega}\right)\right.$$
$$\left.\times\langle\varphi_\kappa|d_\gamma^*|\ \varphi_\beta\rangle\langle\varphi_\beta|d_{\gamma'}|\ \varphi_\kappa\rangle\right\}. \tag{A.3}$$

When we calculation the equation (A.3), we should first rewrite all the corresponding molecular states in a basis of Hunds case (a) state, which is labeled $|\chi;\ J,\ I,\ F,\ M_F\rangle$, where $|\chi\rangle = |\eta,\ v,\ \Lambda;\ S,\ \Sigma,\ \Omega\rangle$, and the quantum number η is used to distinguish the electronic states with the same value of Λ but different energies. Now we convert the nominal basis sets $|X;\ N,\ S,\ J(F)\rangle$ and $|A;\ |\Lambda|,J,\ \pm\rangle$ into basis $|\chi;\ J,\ I,\ F,\ M_F\rangle$ [51]

$$|\Lambda; N, S, J(F)\rangle = \sum_{\Omega}\sum_{\Sigma}(-1)^{J-\Sigma+\Lambda}\sqrt{2N+1} \times \begin{pmatrix} J & S & N \\ \Omega & -\Sigma & -\Lambda \end{pmatrix}|\chi; J, I, F, M_F\rangle, \tag{A.4}$$

while for the *A* state

$$||\Lambda|J, \pm\rangle = \frac{1}{\sqrt{2}}(|\eta, v, \Lambda; S, \Sigma, \Omega; J, I, F, M_F\rangle \pm (-1)^{J-S}|\eta, v, -\Lambda; S, -\Sigma, -\Omega; J, I, F, M_F\rangle). \tag{A.5}$$

Then we calculate the AC Stark shift of the specific $|\varphi_\kappa\rangle$ in $X^2\Sigma^+$ state. We assume that the time-dependent electric field oscillating along the *Z*-axis, i.e. with $\hat{\epsilon} = \hat{Z}$. Equation (A.3) then turn into the following expression:

$$U_\kappa = \Delta E_\kappa = -\frac{\xi^2}{4}\langle\varphi_\kappa|\alpha_{z,z'}|\ \varphi_\kappa\rangle = -\frac{\xi^2}{4}\sum_\beta\left\{\left(\frac{1}{\epsilon_\kappa - \epsilon_\beta - \hbar\omega} + \frac{1}{\epsilon_\kappa - \epsilon_\beta + \hbar\omega}\right)\right.$$
$$\left. \times \langle\varphi_\kappa|T_0^1(d) * |\varphi_\beta\rangle\langle\varphi_\beta|\ T_0^1(d)|\varphi_\kappa\rangle\right\}. \tag{A.6}$$

When we handle the sum in equation (A.6) in Hund case (a) basis, we will split the sum over the $\eta', v', \Lambda', \Sigma',$ Ω', J', F', M_F' into four parts: (a) The sum over the terms diagonal in η, v, Λ, yielding the rotational polarizability α^r. (b) The sum over the terms diagonal in η and Λ but off-diagonal in v, yielding the vibrational polarizability α^v. (c) The sum over the terms diagonal in Λ but off-diagonal in η, yielding the electronic polarizability parallel to the internuclear axis $\alpha^e_\parallel$, referred to the excited Σ state here. (d) The sum over the terms off-diagonal in η and Λ, yielding the electronic polarizability perpendicular to the internuclear axis $\alpha^e_\perp$, referred to the excited Π state here.

Now we first derive α^r as follows. We get the target state $|\varphi_\kappa\rangle$, and other related rotational states $|\varphi_\beta\rangle^r$ coupled to $|\varphi_\kappa\rangle$,

$$|\varphi_\beta\rangle^r = \left|\ \eta, \Lambda = 0; N', S = \frac{1}{2}, J', F'\right\rangle = \sum_{\Omega'}\sum_{\Sigma'}(-1)^{J'-\Sigma'+\Lambda}\sqrt{2N'+1}$$
$$\times \begin{pmatrix} J' & S & N' \\ \Omega' & -\Sigma' & -\Lambda \end{pmatrix}|\chi'; J', I, F', M_F'\rangle. \tag{A.7}$$

Substituting $|\varphi_\kappa\rangle$ and $|\varphi_\beta\rangle^r$ into equation (A.6), we obtain

$$\Delta E_\kappa^r = -\frac{\xi^2}{4}\alpha^r, \quad \alpha^r = \sum_{J'F'M_F'N'\neq N}\sum\left(\frac{1}{\epsilon_{\eta\Lambda vN'J'F'} - \epsilon_{\eta\Lambda vNJF} - \hbar\omega} + \frac{1}{\epsilon_{\eta\Lambda vN'J'F'} - \epsilon_{\eta\Lambda vNJF} + \hbar\omega}\right) \times (C^r)^2, \tag{A.8}$$

where

$$C^r = \sum_{\Sigma'=\Sigma}(-1)^{J'-\Sigma'+J-\Sigma}\sqrt{2N'+1}\sqrt{2N+1}\begin{pmatrix} J' & S & N' \\ \Omega' & -\Sigma' & 0 \end{pmatrix}\begin{pmatrix} J & S & N \\ \Omega & -\Sigma & 0 \end{pmatrix}$$
$$\times \langle\chi'; J', I, F', M_F'|T_0^1(d)|\ \chi; J, I, F, M_F\rangle. \tag{A.9}$$

The last term in equation (A.9) is the matrix element for the electric dipole transition, which can be calculated as follows,

$$\langle d\rangle = \langle\chi'; J', I, F', M_F'|T_0^1(d)|\ \chi; J, I, F, M_F\rangle$$
$$= (-1)^{F'-M_F'+F+J'+I+1}\sqrt{(2F'+1)(2F+1)}\begin{pmatrix} F' & 1 & F \\ -M_F' & 0 & M_F \end{pmatrix}$$
$$\times \begin{Bmatrix} J & F & I \\ F' & J' & 1 \end{Bmatrix}\langle\chi'; J'\|T^1(d)\|\ \chi; J\rangle, \tag{A.10}$$

where the term with brackets and curly brackets are the 3*j*- and 6*j*-symbol respectively.

Applying the Wigner–Eckart theorem to the last term in equation (A.10), we obtain

$$\langle\chi'; J'\|T^1(d)\|\ \chi; J'\rangle = \sum_{q=-1}^1(-1)^{J'-\Omega'}\sqrt{(2J'+1)(2J+1)}\begin{pmatrix} J' & 1 & J \\ -\Omega' & q & \Omega \end{pmatrix}$$
$$\times \langle\eta'v'|\eta v\rangle\langle\Lambda', S, \Sigma'|d|\Lambda, S, \Sigma\rangle. \tag{A.11}$$

Since the electrical dipole operator $T_p^1(d)$ can not change neither the electron spin nor the spin projection, equation (A.11) differs from zero only if $\Sigma' = \Sigma$. Till now, we have obtained the rotational polarizability α^r. The derivation of vibrational polarizability α^v and electronic polarizability $\alpha^e_\parallel$, $\alpha^e_\perp$ is in the same way. However, when we calculate $\alpha^e_\perp$, we only consider the contribution of $A^2\Pi_{1/2}(J' = 1/2(e))$ state, which is the one of negative

parity. Omitting the quantum number η and ν, it is

$$|\varphi_\beta\rangle = \frac{1}{\sqrt{2}}\left(\left|1, \frac{1}{2}, -\frac{1}{2}, \frac{1}{2}, \frac{1}{2}, I, F', M'_F\right\rangle + \left|-1, \frac{1}{2}, -\frac{1}{2}, -\frac{1}{2}, \frac{1}{2}, I, F', M'_F\right\rangle\right). \tag{A.12}$$

Then, α^r, α^v, $\alpha^e_\parallel$ and $\alpha^e_\perp$ are directly given as follows,

$$\alpha^r = \sum_{N'J'F'M'_F}\left(\frac{1}{\mathcal{E}_{\eta\Lambda\nu N'J'F'} - \mathcal{E}_{\eta\Lambda\nu NJF} - \hbar\omega} + \frac{1}{\mathcal{E}_{\eta\Lambda\nu N'J'F'} - \mathcal{E}_{\eta\Lambda\nu NJF} + \hbar\omega}\right) \times (C^r)^2$$

$$C^r = \sum_{\Sigma'=\Sigma}(-1)^{J'-\Sigma'+J-\Sigma}\sqrt{2N'+1}\sqrt{2N+1}\begin{pmatrix}J' & S & N' \\ \Omega' & -\Sigma' & 0\end{pmatrix}\begin{pmatrix}J & S & N \\ \Omega & -\Sigma & 0\end{pmatrix}$$

$$\times (-1)^{F'-M'_F+F+J'+I+1}\sqrt{(2F'+1)(2F+1)} \times \begin{pmatrix}F' & 1 & F \\ -M'_F & 0 & M_F\end{pmatrix}$$

$$\times \begin{Bmatrix}J & F & I \\ F' & J' & 1\end{Bmatrix} \times \sum_{q=-1}^{1}(-1)^{J'-\Omega'}\sqrt{(2J'+1)(2J+1)}$$

$$\times \begin{pmatrix}J' & 1 & J \\ -\Omega' & q & \Omega\end{pmatrix}\langle\eta\nu|\eta\nu\rangle\langle\Lambda, S, \Sigma'|d|\Lambda, S, \Sigma\rangle, \tag{A.13}$$

$$\alpha^v = \sum_{N'J'F'M'_F\nu'\neq\nu}\sum\left(\frac{1}{\mathcal{E}_{\eta\Lambda\nu' N'J'F'} - \mathcal{E}_{\eta\Lambda\nu NJF} - \hbar\omega} + \frac{1}{\mathcal{E}_{\eta\Lambda\nu' N'J'F'} - \mathcal{E}_{\eta\Lambda\nu NJF} + \hbar\omega}\right) \times (C^v)^2$$

$$C^v = \sum_{\Sigma'=\Sigma}(-1)^{J'-\Sigma'+J-\Sigma}\sqrt{2N'+1}\sqrt{2N+1}\begin{pmatrix}J' & S & N' \\ \Omega' & -\Sigma' & 0\end{pmatrix}\begin{pmatrix}J & S & N \\ \Omega & -\Sigma & 0\end{pmatrix}$$

$$\times (-1)^{F'-M'_F+F+J'+I+1}\sqrt{(2F'+1)(2F+1)} \times \begin{pmatrix}F' & 1 & F \\ -M'_F & 0 & M_F\end{pmatrix}$$

$$\times \begin{Bmatrix}J & F & I \\ F' & J' & 1\end{Bmatrix} \times \sum_{q=-1}^{1}(-1)^{J'-\Omega'}\sqrt{(2J'+1)(2J+1)}\begin{pmatrix}J' & 1 & J \\ -\Omega' & q & \Omega\end{pmatrix}$$

$$\times \langle\eta\nu'|\eta\nu\rangle\langle\Lambda, S, \Sigma'|d|\Lambda, S, \Sigma\rangle, \tag{A.14}$$

$$\alpha^e_\parallel = \sum_{\nu'N'J'F'M'_F\eta'\neq\eta}\sum\left(\frac{1}{\mathcal{E}_{\eta'\Lambda\nu' N'J'F'} - \mathcal{E}_{\eta\Lambda\nu NJF} - \hbar\omega} + \frac{1}{\mathcal{E}_{\eta'\Lambda\nu' N'J'F'} - \mathcal{E}_{\eta\Lambda\nu NJF} + \hbar\omega}\right) \times (C^e_\parallel)^2$$

$$C^e_\parallel = \sum_{\Sigma'=\Sigma}(-1)^{J'-\Sigma'+J-\Sigma}\sqrt{2N'+1}\sqrt{2N+1}\begin{pmatrix}J' & S & N' \\ \Omega' & -\Sigma' & 0\end{pmatrix}\begin{pmatrix}J & S & N \\ \Omega & -\Sigma & 0\end{pmatrix}$$

$$\times (-1)^{F'-M'_F+F+J'+I+1}\sqrt{(2F'+1)(2F+1)} \times \begin{pmatrix}F' & 1 & F \\ -M'_F & 0 & M_F\end{pmatrix}$$

$$\times \begin{Bmatrix}J & F & I \\ F' & J' & 1\end{Bmatrix} \times \sum_{q=-1}^{1}(-1)^{J'-\Omega'}\sqrt{(2J'+1)(2J+1)}\begin{pmatrix}J' & 1 & J \\ -\Omega' & q & \Omega\end{pmatrix}$$

$$\times \langle\eta'\nu'|\eta\nu\rangle\langle\Lambda, S, \Sigma'|d|\Lambda, S, \Sigma\rangle. \tag{A.15}$$

$$\alpha^e_\perp = \sum_{\nu'J'F'M'_F\eta'\neq\eta}\sum_{\Lambda'\neq\Lambda}\sum\left(\frac{1}{\mathcal{E}_{\eta'\Lambda'\nu'J'F'} - \mathcal{E}_{\eta\Lambda\nu NJF} - \hbar\omega} + \frac{1}{\mathcal{E}_{\eta'\Lambda'\nu'J'F'} - \mathcal{E}_{\eta\Lambda\nu NJF} + \hbar\omega}\right) \times (C^e_\perp)^2$$

$$C^e_\perp = \sum_{\Sigma'=\Sigma}(-1)^{J-\Sigma}\frac{1}{\sqrt{2}}\sqrt{2N+1}\begin{pmatrix}J & S & N \\ \Omega & -\Sigma & 0\end{pmatrix}(-1)^{F'-M'_F+F+J'+I+1}\sqrt{(2F'+1)(2F+1)}$$

$$\times \begin{pmatrix}F' & 1 & F \\ -M'_F & 0 & M_F\end{pmatrix}\begin{Bmatrix}J & F & I \\ F' & J' & 1\end{Bmatrix}\sum_{q=-1}^{1}(-1)^{J'-\Omega'}\sqrt{(2J'+1)(2J+1)}$$

$$\times \begin{pmatrix}J' & 1 & J \\ -\Omega' & q & \Omega\end{pmatrix}\langle\eta'\nu'|\eta\nu\rangle\langle\Lambda', S, \Sigma'|d|\Lambda, S, \Sigma\rangle. \tag{A.16}$$

For α^r and α^v, the term $<\Lambda, S, \Sigma'|d|\Lambda, S, \Sigma>$ is the dipole moment of the X$^2\Sigma$ state, which is $\sim$2.59 Debye for MgF [52]. The transition moment for the states X$^2\Sigma^+$ and A$^2\Pi$ of the MgF is $\sim$4.62 Debye [52]. While calculating the polarizabilities, we should notice that the term $\langle\eta\nu'|\eta\nu\rangle$ of α^v denotes the vibrational transition within an electronic state [53], which differs from zero only if $\Delta\nu = \pm 1$ for heteronuclear diatomic molecule. The term $\langle\eta'\nu'|\eta\nu\rangle$ of $\alpha^e_\parallel$ and $\alpha^e_\perp$ denotes the FCFs.

Figure A1. AC Stark shift of $|1, n\rangle$ and $|2, n\rangle$ dressed state versus laser detuning at the light intensity I_0, which is the maximum light intensity of the LHB. The LHB power is 500 mW with the waist radius of 0.2 mm. The dash dot lines are the approximate two-level results, and the solid lines are the actually calculated results.
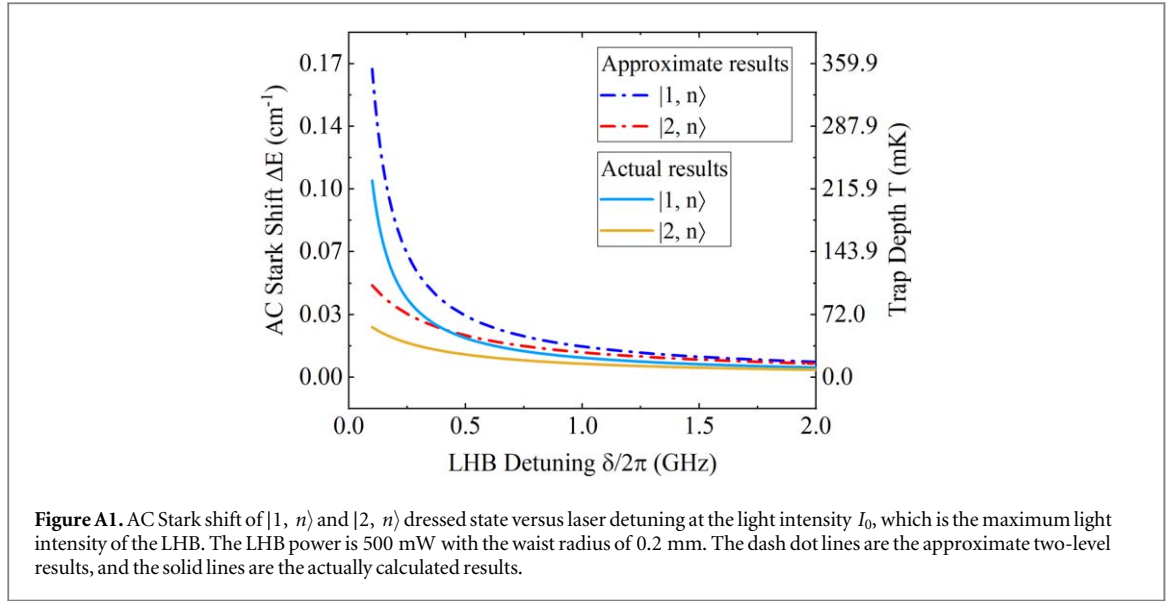
The AC Stark shift of a specific state $|\varphi_\kappa\rangle$ in $X^2\Sigma^+$ thus can be given by

$$U_\kappa = \Delta E_\kappa = -\frac{\xi^2}{4}(\alpha^r + \alpha^v + \alpha^e_{\parallel} + \alpha^e_{\perp}). \tag{A.17}$$

Before we use equation (A.17) to calculate the energy shift of $X^2\Sigma^+(N = 1, F)$, we should notice that with the molecular constants for MgF listed in [54], $|F = 1^-\rangle$ and $|F = 1^+\rangle$ states are

$$|F = 1^-, M_F\rangle = -0.7151|J = 3/2, F = 1, M_F\rangle + 0.6990|J = 1/2, F = 1, M_F\rangle,$$
$$|F = 1^+, M_F\rangle = 0.6990|J = 3/2, F = 1, M_F\rangle + 0.7151|J = 1/2, F = 1, M_F\rangle, \tag{A.18}$$

respectively. Equation (A.18) will be applied to the calculations of all the polarizability.

The relative contributions of the polarizabilities depend on the frequency of the light field, which determines the magnitude of the denominators in equations (A.13)–(A.16). When the wavelength is 359.3 nm, the magnitude of α^r, α^v, $\alpha^e_{\parallel}$ and $\alpha^e_{\perp}$ are $\sim 10^{-44}$, $\sim 10^{-42}$, $\sim 10^{-39}$ and $\sim 10^{-34}$, respectively, where the unit is $C \cdot m^2 V^{-1}$. Hence, the contribution of α^r, α^v and $\alpha^e_{\parallel}$ can be neglected.

After we calculate $U_\kappa = -\xi^2\alpha^e_{\perp}/4$, we finally get the optical potentials of dressed-states of MgF, which shown in figure A1. After we neglect the effect of $|F = 0\rangle$ state, the $|F = 1^-\rangle$ will be adiabatically evolved into the dressed state $|1, n\rangle$ while the $|F = 1^+, 2\rangle$ states, who shares the same AC Stark shift, will be adiabatically evolved into $|2, n\rangle$. We also compare the actually calculated AC Stark shifts with the approximate two-level expressions from [32, 36],

$$U_1 = \frac{\hbar\Gamma^2 I}{12\delta I_{sat}}, \tag{A.19}$$

$$U_2 = \frac{\hbar\Gamma^2 I}{12(\delta + \delta_{hfs})I_{sat}}, \tag{A.20}$$

where δ is the detuning of the LHB, $\delta_{hfs} = 234.7$ MHz is the level splitting between the two ground states for our model, $I_{sat} = (\pi hc\Gamma)/(3\lambda^3)$ and Γ are the saturation intensity and the spontaneous decay rate, respectively. As shown in figure A1, we find that the energy shifts derived from equations (A.19), (A.20) is larger than the actual results, because the complex energy level structures of MgF internal states are not considered.

For MgF molecules, the U of the $|1, n\rangle$ state is much larger than that of the $|2, n\rangle$ state, which is necessary for efficient Sisyphus cooling in the LHB. We should notice that the AC Stark shift plotted in the diagram is the value in the case of the maximum light intensity I_0 of the LHB, and the U of dressed states varies spatially because of the light intensity distribution of the LHB.

Appendix B

In this paper, we calculated the decay factors q_{LHB} and q_{RPB} between the dressed states. For $^{24}Mg^{19}F$ radical, as discussed in the paper, we neglect the $|N = 1, F = 0\rangle$ state, and regard $|N = 1, F = 1^+, 2\rangle$ states as a degenerate state in the case of large detuning. Thus, the hyperfine ground states $|J = 1/2, F = 1^-\rangle$ and $|J = 3/2, F = 1^+, 2\rangle$ in $X^2\Sigma^+(v = 0, N = 1)$ and excited state $|N' = 0, J_u = 1/2\rangle$ in $A^2\Pi_{1/2}(v' = 0)$

constitute a standard Λ-system. The LHB and the RPB are both linearly polarized, so we only consider π-couplings and transitions ($M_F = M'_F = m$).

We now determine the branching ratio q_{LHB}, which is the mean branching ratio to the lower ground states after scattering a LHB photon. In the case of high intensity light filed, each dressed state energy level is the superposition of all related energy levels, the branching ratio q_{LHB} is indeed different from that in weak light fields. When the molecule feels the LHB increasingly, the Λ system coupling with a main laser photon become into the dressed molecular levels. The $|N = 1, J = 1/2, F = 1, m\rangle$ sublevels in $X^2\Sigma^+$ are coupled to the $|J' = 1/2, F', m\rangle$ sublevels in $A^2\Pi_{1/2}$ with the relative transition strengths $|\zeta_{F'm,Fm}|^2$, where

$$
|\zeta_{F'm,Fm}| = \sum_{\Sigma'=\Sigma} (-1)^{J-\Sigma} \frac{1}{\sqrt{2}} \sqrt{2N+1} \begin{pmatrix} J & S & N \\ \Omega & -\Sigma & 0 \end{pmatrix} (-1)^{F'-m+F+J'+I+1} \sqrt{(2F'+1)(2F+1)}
$$
$$
\times \begin{pmatrix} F' & 1 & F \\ -m & 0 & m \end{pmatrix} \begin{Bmatrix} J & F & I \\ F' & J' & 1 \end{Bmatrix} \sum_q (-1)^{J'-\Omega'} \sqrt{(2J'+1)(2J+1)} \begin{pmatrix} J' & 1 & J \\ -\Omega' & q & \Omega \end{pmatrix}. \tag{B.1}
$$

All sublevels of an excited hyperfine level F' have the same branching ratio [32]

$$
q_{F'} = (2F+1)(2J'+1) \begin{Bmatrix} F & 1 & F' \\ J' & I & J \end{Bmatrix}, \tag{B.2}
$$

to decay into the lower hyperfine ground state. By averaging over the lower hyperfine magnetic sublevels m, one obtains

$$
q_{\text{LHB}} = \frac{1}{2F+1} \sum_{m=-F}^{F} \frac{\sum_{F'} |\zeta_{F'm,Fm}|^2 q_{F'}}{\sum_{F'} |\zeta_{F'm,Fm}|^2}, \tag{B.3}
$$

where $F = 1$, $J = 1/2$. Combining equation (A.18), we can obtain the decay factors $q_{\text{LHB}} \approx 0.497$.

Since the q_{RPB} is the branching ratio into the lower ground state for the excitation of the upper ground state by the RPB, which is a very weak field of light, the result of the branching ratio q_{RPB} can be derived from our previous work [29], which is about 0.369.

ORCID iDs

Bin Wei ⬥ https://orcid.org/0000-0001-7596-0581
Yaling Yin ⬥ https://orcid.org/0000-0003-0174-8988
Yong Xia ⬥ https://orcid.org/0000-0002-7138-406X

References

[1] Doyle J M, Friedrich B, Krems R V and Masnou-Seeuws F 2004 *Eur. Phys. J.* D **31** 149
[2] Carr L D, DeMille D, Krems R V and Ye J 2009 *New J. Phys.* **11** 055049
[3] Jin D S and Ye J 2012 *Chem. Rev.* **112** 4801
[4] Shuman E S, Barry J F and Demille D 2010 *Nature* **467** 820
[5] Norrgard E B, McCarron D J, Steinecker M H, Tarbutt M R and DeMille D 2016 *Phys. Rev. Lett.* **116** 063004
[6] Steinecker M H, McCarron D J, Zhu Y and DeMille D 2016 *ChemPhysChem* **17** 3664
[7] Hummon M T, Yeo M, Stuhl B K, Collopy A L, Xia Y and Ye J 2013 *Phys. Rev. Lett.* **110** 143001
[8] Collopy A L, Ding S, Wu Y, Finneran I A, Anderegg L, Augenbraun B L, Doyle J M and Ye J 2018 *Phys. Rev. Lett.* **121** 213201
[9] Anderegg L *et al* 2017 *Phys. Rev. Lett.* **119** 103201
[10] Kozyryev I, Baum L, Matsuda K, Augenbraun B L, Anderegg L, Sedlack A P and Doyle J M 2017 *Phys. Rev. Lett.* **118** 173201
[11] Zeppenfeld M, Englert B G, Glöckner R, Prehn A, Mielenz M, Sommer C, van Buuren L D, Motsch M and Rempe G 2012 *Nature* **491** 570
[12] Prehn A, Ibrügger M, Glöckner R, Rempe G and Zeppenfeld M 2016 *Phys. Rev. Lett.* **116** 063005
[13] Lim J, Almond J R, Trigatzis M A, Devlin J A, Fitch N J, Sauer B E, Tarbutt M R and Hinds E A 2018 *Phys. Rev. Lett.* **120** 123201
[14] Albrecht R, Scharwaechter M, Sixt T, Hofer L and Langen T 2020 *Phys. Rev.* A **101** 013413
[15] Bu W, Chen T, Lv G and Yan B 2017 *Phys. Rev.* A **95** 032701
[16] Aggarwal P *et al* 2018 *Eur. Phys. J.* D **72** 197
[17] Iwata G Z, McNally R L and Zelevinsky T 2017 *Phys. Rev.* A **96** 022509
[18] Letokhov V S and Minogin V G 1981 *Phys. Rep.* **73** 1
[19] Barry J F, McCarron D J, Norrgard E B, Steinecker M H and DeMille D 2014 *Nature* **512** 286
[20] Tarbutt M R 2015 *New J. Phys.* **17** 015007
[21] Devlin J A and Tarbutt M R 2018 *Phys. Rev.* A **98** 063415
[22] Dalibard J and Cohen-Tannoudji C 1989 *J. Opt. Soc. Am.* B **6** 2023
[23] Ungar P, Weiss D S, Riis E and Chu S 1989 *J. Opt. Soc. Am.* B **6** 2072
[24] Shang S, Sheehy B, Straten P V D and Metcalf H 1990 *Phys. Rev. Lett.* **64** 858
[25] Fernandes D R, Sievers F, Kretzschmar N, Wu S, Salomon C and Chevy F 2012 *Europhys. Lett.* **100** 63001
[26] Truppe S, Williams H J, Hambach M, Caldwell L, Fitch N J, Hinds E A, Sauer B E and Tarbutt M R 2017 *Nat. Phys.* **13** 1173
[27] Cheuk L W, Anderegg L, Augenbraun B L, Bao Y, Burchesky S, Ketterle W and Doyle J M 2018 *Phys. Rev. Lett.* **121** 083201
[28] Caldwell L, Devlin J A, Williams H J, Fitch N J and Tarbutt M R 2019 *Phys. Rev. Lett.* **123** 033202

[29] Yang X, Li C, Yin Y, Xu S, Li X, Xia Y and Yin J 2017 *J. Phys. B: At. Mol. Opt. Phys.* **50** 015001
[30] Galica S E, Aldridge L, McCarron D J, Eyler E E and Gould P L 2018 *Phys. Rev. A* **98** 023408
[31] Kozyryev I, Baum L, Aldridge L, Yu P, Eyler E E and Doyle J M 2018 *Phys. Rev. Lett.* **120** 063205
[32] Söding J, Grimm R and Ovchinnikov Y B 1995 *Opt. Commun.* **119** 652
[33] Kuga T, Torii Y, Shiokawa N, Hirano T, Shimizu Y and Sasada H 1997 *Phys. Rev. Lett.* **78** 4713
[34] Ovchinnikov Y B, Manek I and Grimm R 1997 *Phys. Rev. Lett.* **79** 2225
[35] Yin J, Zhu Y, Jhe W and Wang Z 1998 *Phys. Rev. A* **58** 509
[36] Yin J and Zhu Y 1998 *J. Opt. Soc. Am. B* **15** 2235
[37] Yin Y, Xia Y, Ren R, Du X and Yin J 2015 *J. Phys. B: At. Mol. Opt. Phys.* **48** 195001
[38] Xu L, Yin Y, Wei B, Xia Y and Yin J 2016 *Phys. Rev. A* **93** 013408
[39] Xu S, Xia M, Gu R, Yin Y, Xu L, Xia Y and Yin J 2019 *Phys. Rev. A* **99** 033408
[40] Meng X, Wang Z, Yin Y, Qi Z, Yong X and Yin J 2018 *Laser Phys.* **28** 055001
[41] Wang Q, Hou S, Xu L and Yin J 2016 *Phys. Chem. Chem. Phys.* **18** 5432
[42] Bethlem H L, Crompvoets F M, Jongma R T, van de Meerakker S Y and Meijer G 2002 *Phys. Rev. A* **65** 053416
[43] Petrich W, Anderson M H, Ensher J R and Cornell E A 1995 *Phys. Rev. Lett.* **74** 3352
[44] Riedel J, Hoekstra S, Jäger W, Gilijamse J J, van de Meerakker S Y and Meijer G 2011 *Eur. Phys. J. D* **65** 161
[45] Tarbutt M R, Hudson J J, Sauer B E, Hinds E A, Ryzhov V A, Ryabov V L and Ezhov V F 2002 *J. Phys. B: At. Mol. Opt. Phys.* **35** 5013
[46] Rabey I M 2016 *PhD Thesis* Imperial College, London
[47] Skoff S M 2011 *PhD Thesis* Imperial College, London
[48] Zhelyazkova V 2014 *PhD Thesis* Imperial College, London
[49] Barry J F, Shuman E S and DeMille D 2011 *Phys. Chem. Chem. Phys.* **13** 18936
[50] Krems R V 2019 *Molecules in Electromagnetic Fields* (New York: Wiley)
[51] Brown J M and Carrington A 2003 *Rotational Spectroscopy of Diatomic Molcecules* (Cambridge: Cambridge University Press)
[52] Pelegrinia M, Vivacquaa C S, Roberto-Netob O, Ornellasc F R and Machadoa F B C 2005 *Braz. J. Phys.* **35** 950
[53] Demtröder W 2005 *Molecular Physics: Theoretical Principles and Experimental Methods* (New York: Wiley)
[54] Anderson M, Allen M and Ziurys L M 1994 *J. Chem. Phys.* **100** 824